Appl. Math. Mech. -Engl. Ed., **43**(12), 1873–1886 (2022)

APPLIED MATHEMATICS AND MECHANICS (ENGLISH EDITION)

https://doi.org/10.1007/s10483-022-2925-8

Resonance response of fluid-conveying pipe with asymmetric elastic supports coupled to lever-type nonlinear energy sink*

Runqing CAO, Zhijian WANG, Jian ZANG, Yewei ZHANG†

Faculty of Aerospace Engineering, Shenyang Aerospace University, Shenyang 110136, China

(Received May 5, 2022 / Revised Aug. 18, 2022)

Abstract This paper studies the vibration absorber for a fluid-conveying pipe, where the lever-type nonlinear energy sink (LNES) and spring supports are coupled to the asymmetric ends of the system. The pseudo-arc-length method integrated with the harmonic balance method is used to investigate the steady-state responses analytically. Meanwhile, the numerical solution of the fluid-conveying pipe is calculated with the Runge-Kutta method. Moreover, a special response, called the collapsible closed detached response (CCDR), is first observed when the vibration response of mechanical structures is studied. Then, the relationship between the CCDR and the main structure primary response (PR) is obtained. In addition, the closed detached response (CDR) is also observed to research the resonance response of the fluid-conveying pipe. The appearance of either the CCDR or the CDR does affect the resonance attenuation. Furthermore, the mentioned two phenomena underline that the trend of vibration responses under external excitation goes continuous and gradual. Besides, the main advantage of the LNES is presented by contrasting the LNES with the nonlinear energy sink (NES) coupled to the same pipe system. It is found that the LNES can reduce the resonance response amplitude by 91.33%.

Key words fluid-conveying pipe, vibration attenuation, collapsible closed detached response (CCDR), lever-type nonlinear energy sink (LNES), elastic support

Chinese Library Classification O322
2010 Mathematics Subject Classification 74K10

1 Introduction

Flow-induced vibration extensively exists in various forms of fluid-structure interaction machinery, including the wind turbine blades[1], downhole oil pumping systems[2], large offshore platforms[3–4], and others[5–7], and extremely harms the equipment operation. As a representative of fluid-structure interaction systems, the fluid-conveying pipe has drawn many researchers'

* Citation: CAO, R. Q., WANG, Z. J., ZANG, J., and ZHANG, Y. W. Resonance response of fluid-conveying pipe with asymmetric elastic supports coupled to lever-type nonlinear energy sink. *Applied Mathematics and Mechanics* (*English Edition*), **43**(12), 1873–1886 (2022) https://doi.org/10.1007/s10483-022-2925-8

† Corresponding author, E-mail: zhangyewei1218@126.com

Project supported by the National Natural Science Foundation of China (Nos. 11902203 and 12022213) and the General Scientific Research Foundation of Liaoning Educational Committee (No. JYT2020035)

attention[8–11]. They have done considerable work on this classical model[12–14]. For example, some researchers studied the fluid-conveying pipe in three dimensions[15–17]. Pipe models are classified according to the curvature into straight pipes conveying fluid, slightly curved ones[18–19], and curved ones[20].

Meanwhile, various computation approaches and techniques have been developed and used to obtain geometrically exact governing equations[21–23], to investigate the nonlinear dynamics and stability of the system[24–28], and to calculate the resonance response[29]. Other researchers explore the material effects on resonance attenuation[30–31], especially soft materials[32]. Also, some researchers used the energy harvesting method to suppress vibration[33]. Ding et al.[34] focused on the varying boundary conditions of a pipe system in order to isolate resonance. In addition, several researchers devoted themselves to coupling vibration absorbers to pipe models in order to avoid negative vibration[35–37]. Among these mentioned studies, our attention has been paid to two means, namely, diverse boundary conditions and adding vibration absorbers. Because of some practically mechanical devices operated in complicated conditions, the study of complex boundary conditions is helpful for enhancing machinery vibration isolation ability.

Considering convenience and effectiveness for the coupling of vibration absorbers to the main structure, many researchers start their work in view of nonlinearity[38–40]. Among various resonance absorbers, a novel oscillation named as the nonlinear energy sink (NES) has been increasingly popular[41–42]. Owing to strict requirements of aerospace and marine engineering system, several researchers subsequently made many improvements in reducing the attached mass of resonance absorbers and enhancing their vibration control ability[43–44]. Among all forms of NESs, a novel lever-type nonlinear energy sink (LNES)[45] attracts our attention by coupling a dimensionless lever to the NES. The LNES attaches a lightweight mass and achieves the target energy transfer from the main structure. However, in the previous studies, the LNES is applied to the discrete system or the ordinary beam system. The performance of the LNES in the oscillation suppression of the fluid-structure interaction system has not been mentioned yet. Therefore, the LNES coupling to both sides of the fluid-conveying pipe is proposed in this work to avoid undesirable vibration.

Furthermore, some extraordinary phenomena have been found when studying the resonance response of the system under either external excitation or self-excitation. It is called the closed detached response (CDR) or the isolated resonance curve (IRC)[45–46], which always emerges when the bifurcation of the system occurs. However, the previous studies lack an investigation of how the CDR works in the fluid-structure interaction system. It motivates us to explore this mechanism deeply, whether the CDR could appear in the fluid-conveying pipe.

In this paper, a fluid-structure interaction model is established in Section 2. The analysis of free vibration characteristics is reported in Section 3. Both numerical and analytical methods are used to investigate the steady-state response in Section 4. Finally, the conclusions are drawn in Section 5.

2 Dynamic model

The dynamic model of a fluid-conveying pipe with elastic boundary conditions is established in Fig. 1. X, T, V, and U are the coordinates of axial motion distance, time, axial displacement, and transverse displacement, respectively. L denotes the length of the entire pipe. F represents the axial distributed external force. Moreover, K_1, K_3, C_1, and m_1 are referred to as the vertical supported spring at the left end of the pipe, the cubic nonlinear stiffness, the linear damper, and an attached mass at the left LNES. K_2, K_4, C_2, and m_2 are the corresponding variables on the other side. Γ is the fluid velocity, and D and d denote the diameters of the outer and inner pipe, respectively (see Fig. 1).

According to the Hamilton principle, the kinetic energy of the system T_{E} is provided as

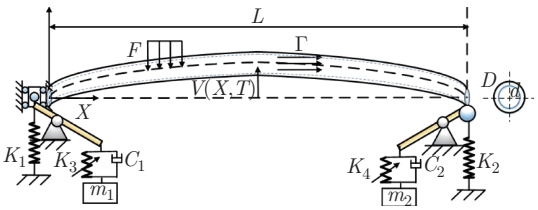

Fig. 1 Mechanical structure of fluid-conveying pipe with LNES (color online)

below,

$$\begin{cases} T_{\mathrm{F}} = \dfrac{1}{2}\displaystyle\int_0^L A_{\mathrm{F}}\rho_{\mathrm{F}}\Big(\Gamma + \frac{\mathrm{d}U}{\mathrm{d}T}\Big)^2\mathrm{d}X + \frac{1}{2}\int_0^L A_{\mathrm{F}}\rho_{\mathrm{F}}\Big(\frac{\mathrm{d}V}{\mathrm{d}T}\Big)^2\mathrm{d}X \\ \quad = \dfrac{1}{2}\displaystyle\int_0^L A_{\mathrm{F}}\rho_{\mathrm{F}}(\Gamma + U_{,T} + \Gamma U_{,X})^2\mathrm{d}X + \frac{1}{2}\int_0^L A_{\mathrm{F}}\rho_{\mathrm{F}}(V_{,T})^2\mathrm{d}X, \\ T_{\mathrm{P}} = \dfrac{1}{2}\displaystyle\int_0^L A_{\mathrm{P}}\rho_{\mathrm{P}}\Big(\frac{\partial U}{\partial T}\Big)^2\mathrm{d}X + \frac{1}{2}\int_0^L A_{\mathrm{P}}\rho_{\mathrm{P}}\Big(\frac{\partial V}{\partial T}\Big)^2\mathrm{d}X \\ \quad = \dfrac{1}{2}\displaystyle\int_0^L A_{\mathrm{P}}\rho_{\mathrm{P}}(U_{,T})^2\mathrm{d}X + \frac{1}{2}\int_0^L A_{\mathrm{P}}\rho_{\mathrm{P}}(V_{,T})^2\mathrm{d}X, \\ T_{\mathrm{E}} = T_{\mathrm{F}} + T_{\mathrm{P}} = \dfrac{1}{2}\displaystyle\int_0^L A_{\mathrm{F}}\rho_{\mathrm{F}}(\Gamma + U_{,T} + \Gamma U_{,X})^2\mathrm{d}X + \frac{1}{2}\int_0^L A_{\mathrm{F}}\rho_{\mathrm{F}}(V_{,T})^2\mathrm{d}X \\ \qquad + \dfrac{1}{2}\displaystyle\int_0^L A_{\mathrm{P}}\rho_{\mathrm{P}}(U_{,T})^2\mathrm{d}X + \frac{1}{2}\int_0^L A_{\mathrm{P}}\rho_{\mathrm{P}}(V_{,T})^2\mathrm{d}X, \end{cases} \tag{1}$$

where T_{F} and T_{P} are the virtual kinetic energies of fluid and pipe, respectively. A_{F} and A_{P} stand for the cross-sectional areas of fluid and pipe, respectively, and ρ_{F} and ρ_{P} denote the densities of fluid and pipe, respectively. Meanwhile, the subscripts ",", T, and X are the partial derivative symbol, partial derivatives of time and axial motion coordinate, respectively. $V_{,X}$ indicates the derivative of V, which represents the first-order derivative with respect to the axial motion coordinate. $V_{,T}$ denotes the first-order derivative of V with respect to time.

According to the Kelvin viscoelastic constitution relation, the material characteristic can be written as[34]

$$\sigma = E\varepsilon + \zeta\varepsilon_{,T}. \tag{2}$$

Then, the potential energy of the pipe can be written as

$$U_{\mathrm{P}} = \iiint_V \sigma\varepsilon\mathrm{d}V. \tag{3}$$

The potential energy of fluid can be written as

$$\begin{aligned} U_{\mathrm{F}} &= \int_0^L A_{\mathrm{F}}P_{\mathrm{F}}(\sqrt{(\mathrm{d}X + \mathrm{d}U)^2 + (\mathrm{d}V)^2} - \mathrm{d}X) \\ &= \int_0^L A_{\mathrm{F}}P_{\mathrm{F}}(\sqrt{(\mathrm{d}X + U_{,X}\mathrm{d}X)^2 + (V_{,X}\mathrm{d}X)^2} - \mathrm{d}X) \\ &= \int_0^L A_{\mathrm{F}}P_{\mathrm{F}}(\sqrt{(1 + U_{,X})^2 + V_{,X}^2} - 1)\mathrm{d}X, \end{aligned} \tag{4}$$

where P_{F} is the pressure of a fluid-conveying element.

Thus, the potential energy of the system is

$$U = U_{\mathrm{F}} + U_{\mathrm{P}}. \tag{5}$$

Then, the virtual work is provided as

$$\begin{aligned}\delta W_1 =& K_1 V(0,T)\delta V(0,T) + K_2 V(L,T)\delta V(L,T)\\ &+ F_1\delta V(0,T) + F_2\delta V(L,T) + F\delta V(X,T),\end{aligned} \tag{6}$$

where

$$\begin{cases} F = F_0\cos(\omega T),\\ F_1 = (\alpha-1)\Big(K_3((\alpha-1)\delta V(0,T)x_1 - x_3)^3 + C_1\Big((\alpha-1)\delta V(0,T)\dfrac{\mathrm{d}x_1}{\mathrm{d}T} - \dfrac{\mathrm{d}x_3}{\mathrm{d}T}\Big)\Big),\\ F_2 = (\alpha-1)\Big(K_4((\alpha-1)\delta V(L,T)x_2 - x_4)^3 + C_2\Big((\alpha-1)\delta V(L,T)\dfrac{\mathrm{d}x_2}{\mathrm{d}T} - \dfrac{\mathrm{d}x_4}{\mathrm{d}T}\Big)\Big), \end{cases} \tag{7}$$

where x_1, x_2, x_3, and x_4 denote the displacement responses of m_1, m_2, left, and right sides of the pipe, respectively. α is the lever fulcrum location parameter. ω and F_0 represent the frequency and the amplitude, respectively. We substitute Eqs. (1)–(7) into the Hamilton principle to obtain the dynamic governing equations and the boundary conditions,

$$\begin{cases} (\rho_{\mathrm{F}}A_{\mathrm{F}} + \rho_{\mathrm{P}}A_{\mathrm{P}})V_{,TT} + (\rho_{\mathrm{F}}A_{\mathrm{F}}\Gamma^2 - A_{\mathrm{F}}P_{\mathrm{F}})V_{,XX} + 2\rho_{\mathrm{F}}A_{\mathrm{F}}\Gamma V_{,XT}\\ \quad + EIV_{,XXXX} + \xi IV_{,XXXXT} + F_0\cos(\omega T) + F_1\delta(X-0) + F_2\delta(X-L) = 0,\\ F_1 = (\alpha-1)\Big(K_3((\alpha-1)\delta V(0,T)x_1 - x_3)^3 + C_1\Big((\alpha-1)\delta V(0,T)\dfrac{\mathrm{d}x_1}{\mathrm{d}T} - \dfrac{\mathrm{d}x_3}{\mathrm{d}T}\Big)\Big),\\ F_2 = (\alpha-1)\Big(K_4((\alpha-1)\delta V(L,T)x_2 - x_4)^3 + C_2\Big((\alpha-1)\delta V(L,T)\dfrac{\mathrm{d}x_2}{\mathrm{d}T} - \dfrac{\mathrm{d}x_4}{\mathrm{d}T}\Big)\Big), \end{cases} \tag{8}$$

$$\begin{cases} V_{,X}(0,T) = 0, \quad V_{,XX}(L,T) = 0,\\ (\rho_{\mathrm{F}}A_{\mathrm{F}}\Gamma^2 - A_{\mathrm{F}}P)V_{,X}(0,T) + EIV_{,XXX}(0,T) + K_1V(0,T) = 0,\\ (\rho_{\mathrm{F}}A_{\mathrm{F}}\Gamma^2 - A_{\mathrm{F}}P)V_{,X}(L,T) + EIV_{,XXX}(L,T) - K_2V(L,T) = 0. \end{cases} \tag{9}$$

The dimensionless equations and the corresponding boundary conditions can be derived by introducing the dimensionless variables and parameters,

$$\begin{cases} v_{,tt} + (\gamma^2-\kappa)v_{,xx} + 2\gamma m_{\mathrm{f}}v_{,xt} + f\cos(\omega_{\mathrm{b}}t) + f_1\delta v(0) + f_2\delta v(1) + v_{,xxxx} + \eta v_{,xxxxt} = 0,\\ f_1 = (\alpha-1)\Big(k_3((\alpha-1)\delta v(0)x_1 - x_3)^3 + C_1\Big((\alpha-1)\delta v(0)\dfrac{\mathrm{d}x_1}{\mathrm{d}t} - \dfrac{\mathrm{d}x_3}{\mathrm{d}t}\Big)\Big),\\ f_2 = (\alpha-1)\Big(k_4((\alpha-1)\delta v(1)x_2 - x_4)^3 + C_2\Big((\alpha-1)\delta v(1)\dfrac{\mathrm{d}x_2}{\mathrm{d}t} - \dfrac{\mathrm{d}x_4}{\mathrm{d}t}\Big)\Big), \end{cases} \tag{10}$$

$$\begin{cases} v_{,x}(0,t) = 0, \quad v_{,xx}(1,t) = 0,\\ (\gamma^2-\kappa)v_{,x}(0,t) + v_{,xxx}(0,t) + k_1v(0,t) = 0,\\ (\gamma^2-\kappa)v_{,x}(1,t)v_{,xxx}(1,t) - k_2v(1,t) = 0, \end{cases} \tag{11}$$

where

$$\begin{cases} v \leftrightarrow \dfrac{V}{L}, \quad x \leftrightarrow \dfrac{X}{L}, \quad t \leftrightarrow \dfrac{T}{L^2}\sqrt{\dfrac{EI}{\rho_{\mathrm{F}}A_{\mathrm{F}}+\rho_{\mathrm{P}}A_{\mathrm{P}}}}, \quad \gamma \leftrightarrow \Gamma L\sqrt{\dfrac{\rho_{\mathrm{F}}A_{\mathrm{F}}}{EI}}, \quad f \leftrightarrow \dfrac{F_0L^3}{EI}, \\ k_1 \leftrightarrow \dfrac{K_1L^3}{EI}, \quad k_2 \leftrightarrow \dfrac{K_2L^3}{EI}, \quad k_3 \leftrightarrow \dfrac{K_3L^5}{EI}, \quad k_4 \leftrightarrow \dfrac{K_4L^5}{EI}, \quad \kappa \leftrightarrow \dfrac{A_{\mathrm{F}}P_{\mathrm{F}}L^2}{EI}, \\ \eta \leftrightarrow \dfrac{\zeta}{L^2}\sqrt{\dfrac{1}{EI(\rho_{\mathrm{F}}A_{\mathrm{F}}+\rho_{\mathrm{P}}A_{\mathrm{P}})}}, \quad \omega_{\mathrm{b}} \leftrightarrow \omega L^2\sqrt{\dfrac{\rho_{\mathrm{F}}A_{\mathrm{F}}+\rho_{\mathrm{P}}A_{\mathrm{P}}}{EI}}, \\ m_{\mathrm{f}} \leftrightarrow \sqrt{\dfrac{\rho_{\mathrm{F}}A_{\mathrm{F}}}{\rho_{\mathrm{F}}A_{\mathrm{F}}+\rho_{\mathrm{P}}A_{\mathrm{P}}}}, \quad c_1 \leftrightarrow \dfrac{C_1L^2}{\sqrt{EI(\rho_{\mathrm{F}}A_{\mathrm{F}}+\rho_{\mathrm{P}}A_{\mathrm{P}})}}, \\ c_2 \leftrightarrow \dfrac{C_2L^2}{\sqrt{EI(\rho_{\mathrm{F}}A_{\mathrm{F}}+\rho_{\mathrm{P}}A_{\mathrm{P}})}}, \quad m_1 \leftrightarrow \dfrac{M_1}{\rho_{\mathrm{F}}A_{\mathrm{F}}+\rho_{\mathrm{P}}A_{\mathrm{P}}}, \quad m_2 \leftrightarrow \dfrac{M_2}{\rho_{\mathrm{F}}A_{\mathrm{F}}+\rho_{\mathrm{P}}A_{\mathrm{P}}}. \end{cases} \tag{12}$$

3 Free vibration analysis

By ignoring the terms of nonlinear stiffness, damper, and external excitation[34], the modal functions of the pipe (see Eq. (10)) can be obtained and simplified as

$$v_{,tt} + (\gamma^2 - \kappa)v_{,xx} + 2\gamma m_{\mathrm{f}} v_{,xt} + v_{,xxxx} = 0. \tag{13}$$

Then, the solutions of the transverse vibration are assumed as follows:

$$\begin{cases} v(t,x) = p(t)\phi(x), \\ p(t) = \mathrm{e}^{\mathrm{i}\omega t}, \quad \phi(x) = C_1\mathrm{e}^{\mathrm{i}\beta_1 x} + C_2\mathrm{e}^{\mathrm{i}\beta_2 x} + C_3\mathrm{e}^{\mathrm{i}\beta_3 x} + C_4\mathrm{e}^{\mathrm{i}\beta_4 x}, \end{cases} \tag{14}$$

where p and ϕ stand for the dimensionless coordinate and the modal function of the fluid-conveying pipe, respectively. Moreover, the coefficients of C_1, C_2, C_3, and C_4 (especially, C_1 is a constant value, which is not equal to zero) can be solved by substituting Eq. (14) into Eqs. (11) and (13),

$$\begin{cases} C_1\beta_1 + C_2\beta_2 + C_3\beta_3 + C_4\beta_4 = 0, \\ C_1\mathrm{e}^{\mathrm{i}\beta_1}\beta_1^2 + C_2\mathrm{e}^{\mathrm{i}\beta_2}\beta_2^2 + C_3\mathrm{e}^{\mathrm{i}\beta_3}\beta_3^2 + C_4\mathrm{e}^{\mathrm{i}\beta_4}\beta_4^2 = 0, \\ k_1(C_1 + C_2 + C_3 + C_4) - 3\mathrm{i}(C_1\beta_1^3 + C_2\beta_2^3 + C_3\beta_3^3 + C_4\beta_4^3) = 0, \\ k_2(C_1\mathrm{e}^{\mathrm{i}\beta_1} + C_2\mathrm{e}^{\mathrm{i}\beta_2} + C_3\mathrm{e}^{\mathrm{i}\beta_3} + C_4\mathrm{e}^{\mathrm{i}\beta_4}) + 3\mathrm{i}(C_1\mathrm{e}^{\mathrm{i}\beta_1}\beta_1^3 + C_2\mathrm{e}^{\mathrm{i}\beta_2}\beta_2^3 + C_3\mathrm{e}^{\mathrm{i}\beta_3}\beta_3^3 \\ \quad + C_4\mathrm{e}^{\mathrm{i}\beta_4}\beta_4^3) + \mathrm{i}(\gamma^2 - \kappa)(C_1\mathrm{e}^{\mathrm{i}\beta_1}\beta_1 + C_2\mathrm{e}^{\mathrm{i}\beta_2}\beta_2 + C_3\mathrm{e}^{\mathrm{i}\beta_3}\beta_3 + C_4\mathrm{e}^{\mathrm{i}\beta_4}\beta_4) = 0, \end{cases} \tag{15}$$

$$-\omega^2 - (\gamma^2 - \kappa)\beta_j^2 - 2\gamma m_{\mathrm{f}}\omega\beta_j + \beta_j^4 = 0, \tag{16}$$

where $j = 1$, 2, 3, and 4.

To investigate the dynamical characteristics of the fluid-conveying pipe, the parameters used in the computation are listed in Table 1.

The relationship of the frequency with vertical spring and the fluid speed is illustrated in Fig. 2. It is obvious that the vertical spring stiffness has a limited effect on the frequency. After a surge in the beginning (see Fig. 2(a)), the first four order frequencies vary slowly all the time. Thereafter, the value of vertical spring is selected moderately to avoid harmful vibration. As the fluid speed increases, the curves of first three order frequencies decline until the fluid speed reaches 50 (see Fig. 2(b)). Then, the curve of the first-order frequency changes slightly, while the curves of the third and fourth frequencies are unstable and increase obviously and gradually, indicating that the fluid speed is essential to the characteristics of the system, especially for high order natural frequencies. To deeply explore the effect of the fluid speed, the modal functions of the fluid-conveying pipe are shown in Fig. 3.

Table 1 Parameters of fluid-conveying pipe and LNES

Notation	Value	Notation	Value
E	850 MPa	ρ_{P}	920 kg/m^3
D	0.02 m	K_3, K_4	394.144 2 N/m
d	0.016 m	M_1, M_2	0.030 5 kg
A_{F}	2.011×10^{-4} m^2	C_1, C_2	0.054 8 N/(m·s)
A_{P}	1.131×10^{-4} m^2	α	6
ρ_{F}	1 000 kg/m^3	L	1 m

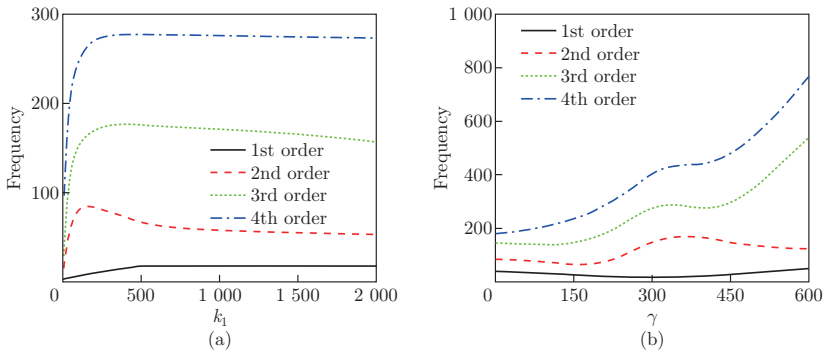

Fig. 2 Frequencies of fluid-conveying pipe versus (a) vertical spring k_1 and (b) fluid speed γ (color online)

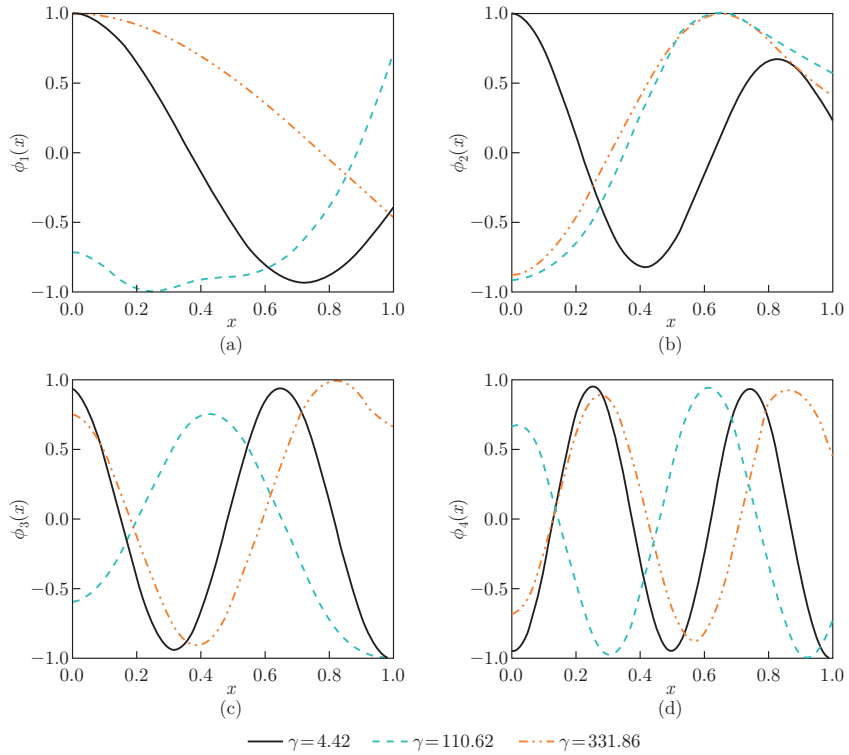

Fig. 3 Modal functions of fluid-conveying pipe for different values of fluid speed γ: (a) 1st order modal function, (b) 2nd order modal function, (c) 3rd order modal function, and (d) 4th order modal function (color online)

4 Forced vibration analysis

To obtain the simplified modal function ϕ used in the Galerkin method, the nonlinear stiffness, damper, external excitation[45], and fluid flow have been ignored. Equations (14) and (15) can be simplified as follows:

$$v_{,tt} + v_{,xxxx} = 0, \tag{17}$$

$$\begin{cases} v_{,x}(0,t) = 0, \quad v_{,xx}(1,t) = 0, \\ v_{,xxx}(0,t) + k_1 v(0,t) = 0, \quad v_{,xxx}(1,t) - k_2 v(1,t) = 0. \end{cases} \tag{18}$$

The dimensionless displacement is assumed as

$$\begin{cases} v(t,s) = p(t)\phi(s), \\ \phi(x) = B_1\cos(\beta x) + B_2\sin(\beta x) + B_3\cosh(\beta x) + B_4\sinh(\beta x), \quad \omega^2 - \beta^4 = 0, \end{cases} \tag{19}$$

where p means the dimensionless transverse coordinate of the pipe system.

In addition, the simplified modal functions ϕ can be expressed in Eq. (19), and the coefficients of simplified modal functions can be obtained by substituting Eq. (19) into Eqs. (17) and (18). Thus, the solution of the forced vibration governing function can be written as

$$v(t,x) = \sum_{i=1}^{n} p_i(t)\phi_i(x), \tag{20}$$

where $i = 1, 2, 3, \cdots, n$, and ϕ_i is equal to the modal function ϕ. Moreover, substitute this form of solutions into Eq. (10), and thus obtain the Galerkin truncation as follows:

$$\begin{cases} \dfrac{\mathrm{d}^2 p(t)}{\mathrm{d}t^2} + W_1\dfrac{\mathrm{d}p(t)}{\mathrm{d}t} + W_2 p(t) + W_3\cos(\omega_{\mathrm{b}} t) + f_1\phi_g(0) + f_2\phi_g(1) = 0, \\ W_1 = \dfrac{2\gamma m_{\mathrm{f}}\int_0^1 \sum\limits_{i=1}^{n}\phi'(x)\phi_g(x)\mathrm{d}x + \eta\int_0^1 \sum\limits_{i=1}^{n}\phi''''(x)\phi_g(x)\mathrm{d}x}{\int_0^1 \sum\limits_{i=1}^{n}\phi(x)\phi_g(x)\mathrm{d}x}, \\ W_2 = \dfrac{(\gamma^2 - \kappa)\int_0^1 \sum\limits_{i=1}^{n}\phi''(x)\phi_g(x)\mathrm{d}x + \int_0^1 \sum\limits_{i=1}^{n}\phi''''(x)\phi_g(x)\mathrm{d}x}{\int_0^1 \sum\limits_{i=1}^{n}\phi(x)\phi_g(x)\mathrm{d}x}, \\ W_3 = \dfrac{\int_0^1 f\phi_g(x)\mathrm{d}x}{\int_0^1 \sum\limits_{i=1}^{n}\phi(x)\phi_g(x)\mathrm{d}x}, \quad g = 1, 2, 3, 4, \end{cases} \tag{21}$$

where the weight function of Galerkin truncation ϕ_g is set as the modal function of the simplified system. The truncation order is selected as 4 to ensure the convergence of the analytical results[34,45]. The vibration attenuation indicator is set as u_{r}, which ensures the movement of the system. It is expressed as follows:

$$u_{\mathrm{r}}(f) = R_{\mathrm{MS}}\Big(\sum_{i=1}^{n} p_i(t)\phi_i(s)\Big), \tag{22}$$

where R_{MS} stands for the root mean square, and f means the given frequency.

The harmonic balance method is always used to obtain the analytical solution[45]. Consider the influence of the cubic stiffness in the LNES. Then, the three-order dimensionless harmonic solution is assumed as follows[45]:

$$q_j = A_{j1}\cos(\omega t) + A_{j2}\sin(\omega t) + A_{j3}\cos(3\omega t) + A_{j4}\sin(3\omega t), \tag{23}$$

where $j = 1$, 2, 3, and 4. Combining the harmonic balance method and the pseudo-arc-length method is useful for studying the analytical solution of the pipe conveying fluid, especially dealing with the multivalued uncertain problem and the turning point problems during computing directional iterative solutions.

It is noticed that the middle point of the pipe is weaker than any other part of the pipe for the model supported at both ends. Thus, the middle point of the pipe is selected to be the evaluation point, which proves whether the proposed scheme can control vibration[45].

To obtain the numerical solution, the fourth-order Runge-Kutta method is applied in this work. Then, the analysis of forced vibration is conducted to study whether the analytical solution matches the numerical solution and is shown as follows.

Figure 4 shows that the numerical and analytical solutions have excellent agreement. It also demonstrates that the two applied approaches for studying the steady-state responses of fluid-conveying pipe are valuable and the results are convergent.

4.1 Effects of fluid speed

The steady-state responses of the pipe conveying fluid with or without the LNES for different fluid speeds are calculated and depicted in Fig. 5. The vibration response of the system coupled with the LNES is always lower than that without the LNES (see red dotted lines) no matter how the fluid speed varies. It proves that the LNES is a robust resonance absorber, which is helpful for reducing the first-order vibration response peak. Therefore, we focus on the resonance response near the first-order vibration peak and explore the effect of the LNES on the resonance suppression as below.

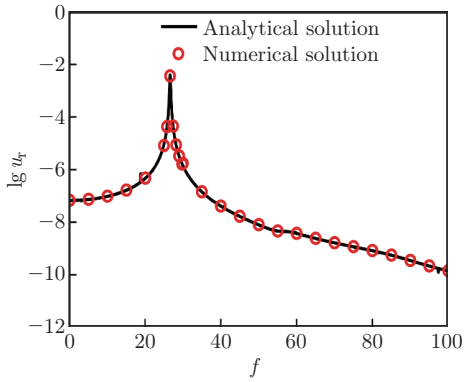

Fig. 4 Steady-state responses of system simulating through analytical and numerical methods (color online)

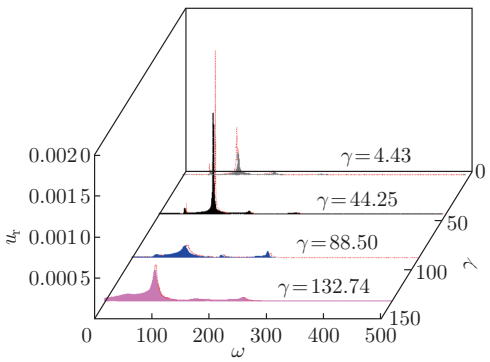

Fig. 5 Resonance responses of u_r changing with fluid speed γ, where dash line denotes NES, solid lines denote LNES with $m_1 = m_2 = 0.1$, $k_3 = 100$, $c_1 = 0.019$, and $\alpha = 6$ (color online)

4.2 Effects of LNES parameters

In this section, we focus on the influence of the LNES on the resonance suppression. After the fluid speed is given, the discussion of the LNES parameters is conducted.

The lever fulcrum α is the ratio of AB to AC, which indicates how the fulcrum location affects the LNES resonance suppression. The LNES is composed of the lever fulcrum α, the cubic nonlinear stiffness k_3, the linear damper c_1, and the linear attached mass m_1 (see Fig. 6).

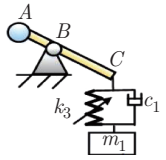

Fig. 6 Structure of LNES (color online)

The effects of lever fulcrum α on resonance control are discussed in Fig. 7. Obviously, the nonlinearity of the fluid-conveying pipe is weak in the initial stage. Then, the primary response (PR) maximum decreases by 61.91%, with α increasing from 3.1 to 4.95 (see Figs. 7(a) and 7(b)). Then, a collapsible closed detached response (CCDR) is observed on the left side of the PR and is depicted with red solid lines. As α increases, the CCDR becomes smaller. Meanwhile, a CDR appears (see Fig. 7(c)). Notably, the PR maximum is almost unchanged from the appearance of the CCDR to the disappearance of the CDR, while the peak of the PR surges after the CDR finally vanishes (see Fig. 7(d)). It can be concluded that the lever fulcrum plays a major role in suppressing vibration. Meanwhile, finding an appropriate range of lever fulcrums is useful for minimizing damaged vibration.

Different from the trend of vibration responses illustrated in Fig. 7, the effect of the attached mass on the resonance suppression is shown in Fig. 8. The resonance peak is high at first (see Fig. 8(a)), then the CDR appears suddenly (see Fig. 8(b)) and gradually becomes higher. After that, the CCDR separates from the PR (see Fig. 8(c)). Finally, the nonlinearity of the system is

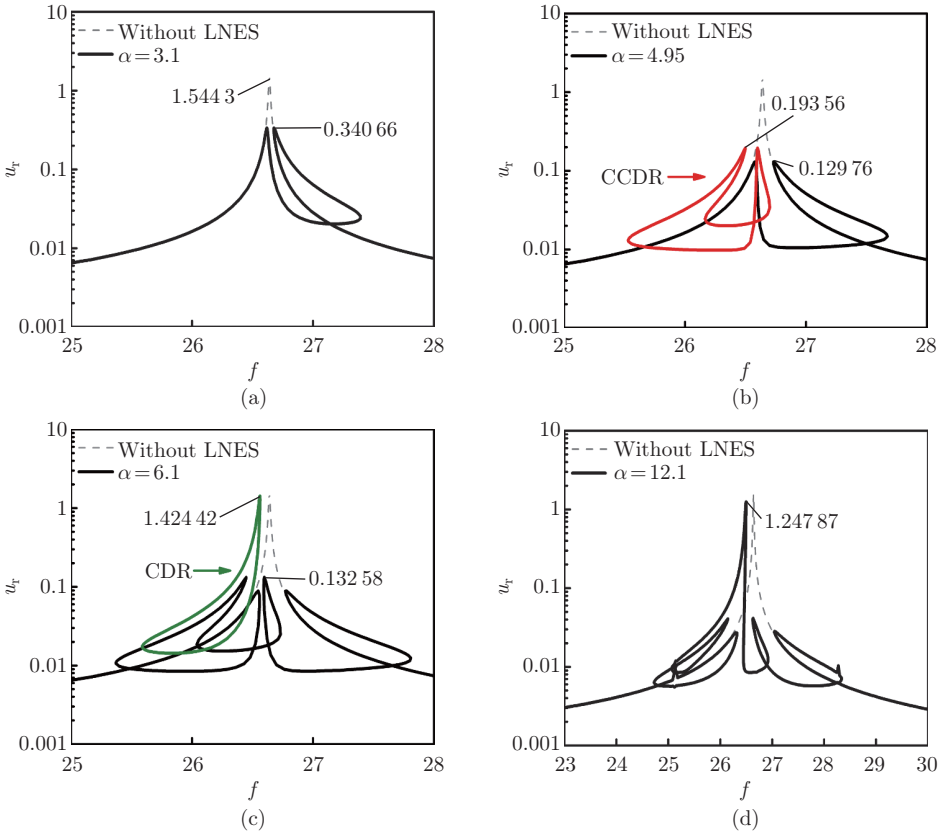

Fig. 7 Resonance responses of u_r for different values of lever fulcrum α: (a) $\alpha = 3.1$, (b) $\alpha = 4.95$, (c) $\alpha = 6.1$, and (d) $\alpha = 12.1$ (color online)

weaker than that in the initial stage and is illustrated in Fig. 8(d). Consequently, the moderate value of an attached mass is effective to the unavoidable vibration control.

The combined effects of the lever fulcrum and the attached mass on the resonance responses are shown in Fig. 9(a). From the projection of the PR (see Fig. 9(c)), it should be noticed that the maximum of u_r drops suddenly, while the appearances of the CDR and the CCDR fill this gap (see Figs. 9(a) and 9(b)). It testifies that the changing trend of the resonance response is continuous. Moreover, it is significant to find an appropriate range of system parameters.

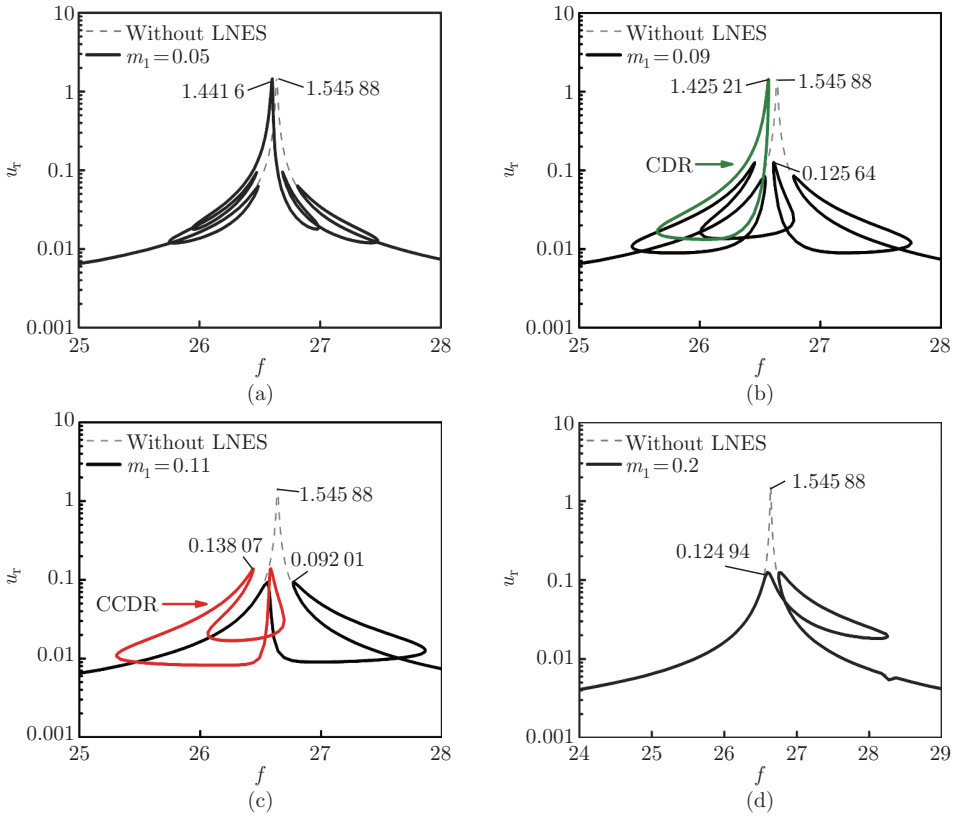

Fig. 8 Resonance responses of u_r for different values of attached mass m_1: (a) $m_1 = 0.05$, (b) $m_1 = 0.09$, (c) $m_1 = 0.11$, and (d) $m_1 = 0.2$ (color online)

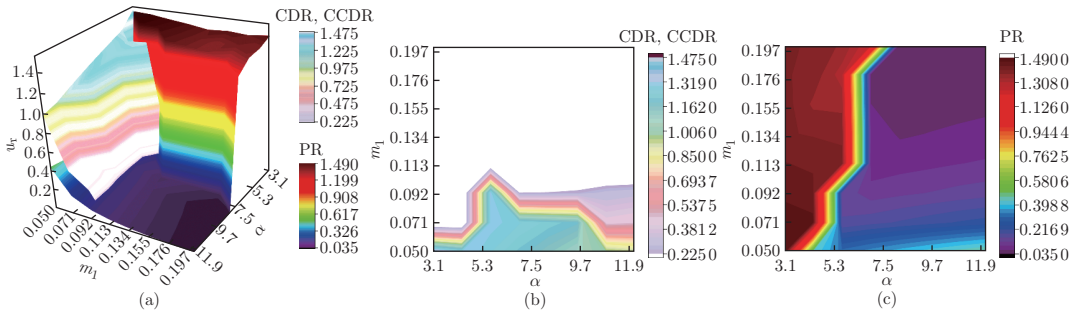

Fig. 9 Maximum resonance responses of u_r changing with lever fulcrum α and attached mass m_1: (a) three-dimensional plot, (b) projection of CDR and CCDR on αm_1-plane, and (c) projection of PR on αm_1-plane (color online)

4.3 Comparison of vibration responses for pipe coupled to LNES and NES

The advantage of the LNES is further discussed by comparing the vibration responses of the same fluid-conveying pipe coupled to the NES. The value of the mass is set as an independent variable when contrasting the vibration control capacity of the LNES with that of the NES. There is no significant difference in the vibration response as shown in Fig. 10(a). Because of the CCDR emergence, the vibration peak of the system with the LNES declines sharply by 91.33% (see Fig. 10(a)), while the response of the system coupled to NES fluctuates slightly (see Figs. 10(b) and 10(c)). Thus, the vibration suppression ability of the LNES is much stronger than that of the NES.

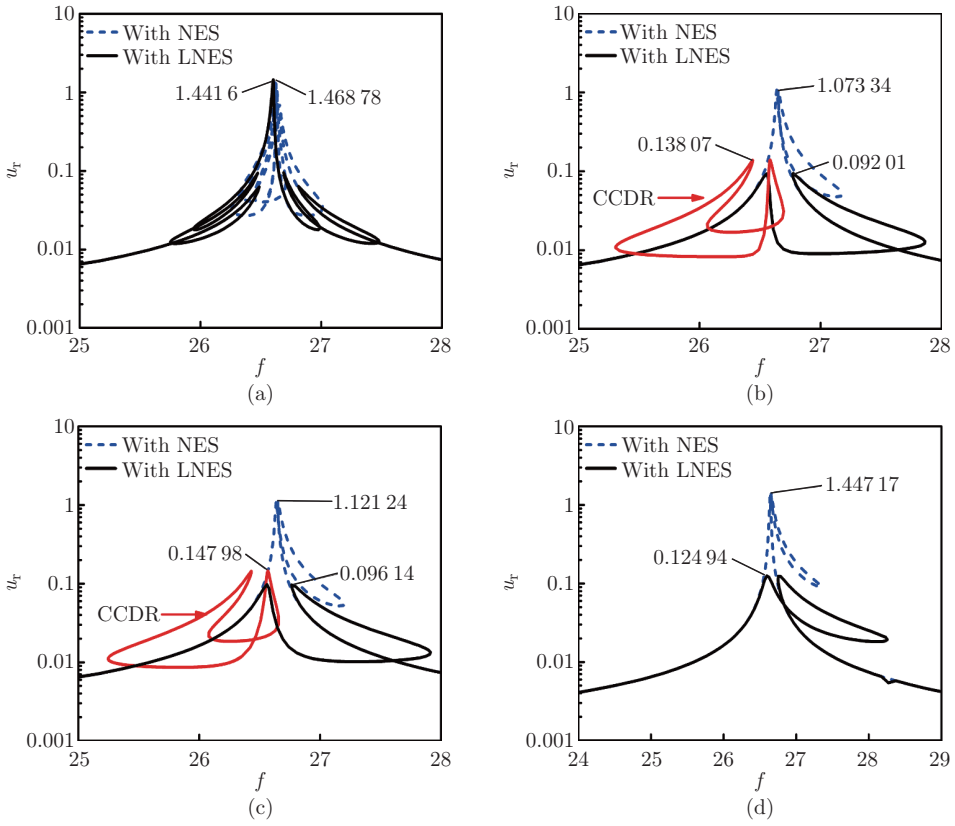

Fig. 10 Resonance responses of u_r for different values of attached mass: (a) $m_1 = 0.05$, (b) $m_1 = 0.11$, (c) $m_1 = 0.12$, and (d) $m_1 = 0.2$ (color online)

5 Conclusions

A novel model of the fluid-conveying pipe is proposed in this work, where the vertical linear spring and the LNES are set as the boundary supports to suppress vibration. The analyses and discussion of the free vibration characteristics and steady-state responses are studied, and important results are obtained as follows:

(i) The fluid speed plays an essential role in exploring the system characteristics, and the high speed always causes negative vibration of the fluid-conveying pipe.

(ii) The appearance of the CCDR when studying forced vibration responses enriches the research of complex vibration responses. Meanwhile, the CDR is also first found when studying the fluid-structure interaction system.

(iii) Both the CDR and the CCDR have been investigated deeply when studying the effects

of the LNES on resonance control. Their appearances or disappearances have dramatically reduced the vibration response peak of the pipe. The appearances of the CCDR and the CDR also demonstrate that the vibration response of the fluid-conveying pipe coupled to the vibration absorber changes gradually but not sharply. Thus, finding an appropriate range of absorber parameters is necessary.

(iv) The LNES is a robust vibration absorber used to suppress the negative resonance of the fluid-conveying pipe than any other classical NESs.

References

[1] DU, Y., ZHOU, S. X., JING, X. J., PENG, Y. P., WU, H. K., and KWOK, N. Damage detection techniques for wind turbine blades: a review. *Mechanical Systems and Signal Processing*, **141**, 106445 (2020)

[2] LI, W. C., VAZIRI, V., APHALE, S. S., DONG, S. M., and WIERCIGROCH, M. Dynamics and frequency and voltage control of downhole oil pumping system. *Mechanical Systems and Signal Processing*, **139**, 106562 (2020)

[3] SUN, K., YI, Y., ZHENG, X. B., CUI, L., ZHAO, C. K., LIU, M. Y., and RAO, X. Experimental investigation of semi-submersible platform combined with point-absorber array. *Energy Conversion and Management*, **245**, 114623 (2021)

[4] ZHANG, Y., WANG, S. Q., FANG, H., HAN, H. W., and XU, Y. H. Design and simulation of a damper with negative stiffness for vibration mitigation from drilling equipment to a semi-submersible platform. *Shock and Vibration*, **2020**, 2605381 (2020)

[5] WANG, S., LIU, Y., and HUANG, W. Research on solid-liquid coupling dynamics of pipe conveying fluid. *Applied Mathematics and Mechanics* (*English Edition*), **19**, 1065–1071 (1998) https://doi.org/10.1007/BF02459195

[6] LI, Z. Y., ZHOU, S. X., and LI, X. A piezoelectric-electromagnetic hybrid flutter-based wind energy harvester: modeling and nonlinear analysis. *International Journal of Non-Linear Mechanics*, **144**, 105051 (2022)

[7] NIU, J. C., HOU, J., SHEN, Y. J., and YANG, S. P. Dynamic analysis and vibration control of nonlinear boring bar with fractional-order model of magnetorheological fluid. *International Journal of Non-Linear Mechanics*, **121**, 103459 (2020)

[8] WADHAM-GAGNON, M., PAÏDOUSSIS, M. P., and SEMLER, C. Dynamics of cantilevered pipes conveying fluid, part 1: nonlinear equations of three-dimensional motion. *Journal of Fluids and Structures*, **23**, 545–567 (2007)

[9] WANG, J. L., YURCHENKO, D., HU, G. B., ZHAO, L. Y., TANG, L. H., and YANG, Y. W. Perspectives in flow-induced vibration energy harvesting. *Applied Physics Letters*, **119**, 100502 (2021)

[10] GIACOBBI, D. B., SEMLER, C., and PAÏDOUSSIS, M. P. Dynamics of pipes conveying fluid of axially varying density. *Journal of Sound and Vibration*, **473**, 115202 (2020)

[11] WANG, Y., WANG, Z., and ZHANG, X. Robust active vibration suppression of single-walled carbon nanotube using adaptive sliding-mode control and electrostatic actuators. *Journal of Vibration and Control* (2022) https://doi.org/10.1177/107754632110630

[12] LU, Z. Q., CHEN, J., DING, H., and CHEN, L. Q. Energy harvesting of a fluid-conveying piezoelectric pipe. *Applied Mathematical Modelling*, **107**, 165–181 (2022)

[13] HONG, J., HE, Z. Z., ZHANG, G. Y., and MI, C. W. Size and temperature effects on band gaps in periodic fluid-filled micropipes. *Applied Mathematics and Mechanics* (*English Edition*), **42**, 1219–1232 (2021) https://doi.org/10.1007/s10483-021-2769-8

[14] GAN, C. B., JING, S., YANG, S. X., and LEI, H. Effects of supported angle on stability and dynamical bifurcations of cantilevered pipe conveying fluid. *Applied Mathematics and Mechanics* (*English Edition*), **36**, 729–746 (2015) https://doi.org/10.1007/s10483-015-1946-6

[15] TANG, Y., XU, J. Y., and YANG, T. Z. Natural dynamic characteristics of a circular cylindrical Timoshenko tube made of three-directional functionally graded material. *Applied Mathematics and Mechanics* (*English Edition*), **43**, 479–496 (2022) https://doi.org/10.1007/s10483-022-2839-6

[16] CHEN, W., DAI, H. L., and WANG, L. Three-dimensional dynamical model for cantilevered pipes conveying fluid under large deformation. *Journal of Fluids and Structures*, **105**, 103329 (2021)

[17] CHEN, W., WANG, L., YAN, Z., and LUO, B. Three-dimensional large-deformation model of hard-magnetic soft beams. *Composite Structures*, **266**, 113822 (2021)

[18] CHEN, W., ZHOU, K., WANG, L., and YIN, Z. P. Geometrically exact model and dynamics of cantilevered curved pipe conveying fluid. *Journal of Sound and Vibration*, **534**, 117074 (2022)

[19] ZHOU, K., NI, Q., CHEN, W., DAI, H. L., PENG, Z. R., and WANG, L. New insight into the stability and dynamics of fluid-conveying supported pipes with small geometric imperfections. *Applied Mathematics and Mechanics* (*English Edition*), **42**, 703–720 (2021) https://doi.org/10.1007/s10483-021-2729-6

[20] LIANG, F., YANG, X. D., ZHANG, W., and QIAN, Y. J. Dynamical modeling and free vibration analysis of spinning pipes conveying fluid with axial deployment. *Journal of Sound and Vibration*, **417**, 65–79 (2018)

[21] CHEN, W., DAI, H. L., JIA, Q. Q., and WANG, L. Geometrically exact equation of motion for large-amplitude oscillation of cantilevered pipe conveying fluid. *Nonlinear Dynamics*, **98**, 2097–2114 (2019)

[22] TAN, X., MAO, X. Y., DING, H., and CHEN, L. Q. Vibration around non-trivial equilibrium of a supercritical Timoshenko pipe conveying fluid. *Journal of Sound and Vibration*, **428**, 104–118 (2018)

[23] LI, M., XU, Q., CHEN, X. C., ZHANG, X. L., and LI, Y. H. Modeling and modal analysis of non-uniform multi-span oil-conveying pipes with elastic foundations and attachments. *Applied Mathematical Modelling*, **88**, 664–675 (2020)

[24] ROUSSELET, J. and HERRMANN, G. Flutter of articulated pipes at finite amplitude. *Journal of Applied Mechanics*, **44**, 154–158 (1977)

[25] BUTT, M. F. J., PAÏDOUSSIS, M. P., and NAHON, M. Dynamics of a confined pipe aspirating fluid and concurrently subjected to external axial flow: theoretical investigation. *Journal of Sound and Vibration*, **509**, 116148 (2021)

[26] TAN, X., DING, H., and CHEN, L. Q. Nonlinear frequencies and forced responses of pipes conveying fluid via a coupled Timoshenko model. *Journal of Sound and Vibration*, **455**, 241–255 (2019)

[27] ZHAO, F. Q., WANG, Z. M., FENG, Z. Y., and LIU, H. Z. Stability analysis of Maxwell viscoelastic pipes conveying fluid with both ends simply supported. *Applied Mathematics and Mechanics* (*English Edition*), **22**, 1436–1445 (2001) https://doi.org/10.1023/A:1022843012114

[28] TANG, Y., WANG, G., and DING, Q. Nonlinear fractional-order dynamic stability of fluid-conveying pipes constituted by the viscoelastic materials with time-dependent velocity. *Acta Mechanica Solida Sinica*, **145**, 1–13 (2022)

[29] ZHANG, Y. F., LIU, T., and ZHANG, W. Nonlinear resonant responses, mode interactions, and multitime periodic and chaotic oscillations of a cantilevered pipe conveying pulsating fluid under external harmonic force. *Complexity*, **2020**, 1–26 (2020)

[30] LU, Z. Q., ZHANG, K. K., DING, H., and CHEN, L. Q. Nonlinear vibration effects on the fatigue life of fluid-conveying pipes composed of axially functionally graded materials. *Nonlinear Dynamics*, **100**, 1091–1104 (2020)

[31] XU, J. and YANG, Q. B. Flow-induced internal resonances and mode exchange in horizontal cantilevered pipe conveying fluid (II). *Applied Mathematics and Mechanics* (*English Edition*), **27**, 943–951 (2006) https://doi.org/10.1007/s10483-006-0710-z

[32] CHEN, W., HU, Z. Y., DAI, H., and WANG, L. Extremely large-amplitude oscillation of soft pipes conveying fluid under gravity. *Applied Mathematics and Mechanics* (*English Edition*), **41**, 1381–1400 (2020) https://doi.org/10.1007/s10483-020-2646-6

[33] LYU, X. F., CHEN, F., REN, Q. Q., TANG, Y., DING, Q., and YANG, T. Z. Ultra-thin piezoelectric lattice for vibration suppression in pipe conveying fluid. *Acta Mechanica Solida Sinica*, **33**, 770–780 (2020)

[34] DING, H., JI, J. C., and CHEN, L. Q. Nonlinear vibration isolation for fluid-conveying pipes using quasi-zero stiffness characteristics. *Mechanical Systems and Signal Processing*, **121**, 675–688 (2019)

[35] ZHOU, K., XIONG, F. R., JIANG, N. B., DAI, H. L., YAN, H., WANG, L., and NI, Q. Nonlinear vibration control of a cantilevered fluid-conveying pipe using the idea of nonlinear energy sink. *Nonlinear Dynamics*, **95**, 1435–1456 (2019)

[36] YANG, T. Z., LIU, T., TANG, Y., HOU, S., and LV, X. F. Enhanced targeted energy transfer for adaptive vibration suppression of pipes conveying fluid. *Nonlinear Dynamics*, **97**, 1937–1944 (2019)

[37] SHOAIB, M., CHEN, Z., and LI, F. M. Vibration attenuation of periodic non-uniform pipes conveying fluid. *Journal of Vibration Engineering & Technologies*, **9**, 2035–2045 (2021)

[38] CHEN, B. C., CHEN, L. M., DU, B., LIU, H. C., LI, W. G., and FANG, D. N. Novel multifunctional negative stiffness mechanical metamaterial structure: tailored functions of multi-stable and compressive mono-stable. *Composites Part B*: *Engineering*, **204**, 108501 (2021)

[39] DING, H. and CHEN, L. Q. Designs, analysis, and applications of nonlinear energy sinks. *Nonlinear Dynamics*, **100**, 3061–3107 (2020)

[40] LIU, Y., MOJAHED, A., BERGMAN, L. A., and VAKAKIS, A. F. A new way to introduce geometrically nonlinear stiffness and damping with an application to vibration suppression. *Nonlinear Dynamics*, **96**, 1819–1845 (2019)

[41] JING, X. J. and VAKAKIS, A. F. Exploring nonlinear benefits in engineering. *Mechanical Systems and Signal Processing*, **125**, 1–3 (2019)

[42] YANG, T., ZHANG, Y. Q., ZHOU, S. X., FAN, H. W., and ZHANG, X. H. Wideband energy harvesting using nonlinear energy sink with bio-inspired hexagonal skeleton structure. *Communications in Nonlinear Science and Numerical Simulation*, **111**, 106465 (2022)

[43] GENG, X. F. and DING, H. Two-modal resonance control with an encapsulated nonlinear energy sink. *Journal of Sound and Vibration*, **520**, 116667 (2022)

[44] WANG, G. X. and DING, H. Mass design of nonlinear energy sinks. *Engineering Structures*, **250**, 113438 (2022)

[45] ZANG, J., CAO, R. Q., and ZHANG, Y. W. Steady-state response of a viscoelastic beam with asymmetric elastic supports coupled to a lever-type nonlinear energy sink. *Nonlinear Dynamics*, **105**, 1327–1341 (2021)

[46] GUO, H. L., YANG, T. Z., CHEN, Y. S., and CHEN, L. Q. Singularity analysis on vibration reduction of a nonlinear energy sink system. *Mechanical Systems and Signal Processing*, **173**, 109074 (2022)